FISEVIER

Contents lists available at ScienceDirect

# Journal of Pharmaceutical Sciences

journal homepage: www.jpharmsci.org



Pharmaceutics, Drug Delivery and Pharmaceutical Technology

# A Rheological Approach for Predicting Physical Stability of Amorphous Solid Dispersions



Sichen Song<sup>a,b</sup>, Chenguang Wang<sup>a</sup>, Bo Zhang<sup>c</sup>, Changquan Calvin Sun<sup>a</sup>, Timothy P. Lodge<sup>c,d</sup>, Ronald A. Siegel<sup>a,e,\*</sup>

- <sup>a</sup> Department of Pharmaceutics, University of Minnesota, Minneapolis, MN 55455, United States
- <sup>b</sup> School of Mathematics, University of Minnesota, Minneapolis, MN 55455, United States
- <sup>c</sup> Department of Chemical Engineering and Materials Science, University of Minnesota, Minneapolis, MN 55455, United States
- <sup>d</sup> Department of Chemistry, University of Minnesota, Minneapolis, MN 55455, United States
- <sup>e</sup> Department of Biomedical Engineering, University of Minnesota, Minneapolis, MN 55455, United States

#### ARTICLE INFO

#### Article history: Received 21 June 2022 Revised 19 August 2022 Accepted 19 August 2022 Available online 26 August 2022

Keywords:
Amorphous solid dispersion (ASD)
Miscibility
Viscosity
Overlap concentration (c\*)
Physical stability
Crystallization

#### ABSTRACT

Miscibility is an important indicator of physical stability against crystallization of amorphous solid dispersions (ASDs). Currently available methods for miscibility determination have both theoretical and practical limitations. Here we report a method of miscibility determination based on the overlap concentration,  $c^*$ , which can be conveniently determined from the viscosity-composition diagram. The determined  $c^*$  values for ASDs of two model drugs, celecoxib and loratadine, with four different grades of polyvinylpyrrolidone (PVP), were correlated strongly with the physical stability of ASDs. This result suggests potential application of the  $c^*$  concept in guiding the design of stable high drug loaded ASD formulations. A procedure is provided to facilitate broader adoption of this methodology. The procedure is easy to apply and widely applicable for thermally stable binary drug/polymer combinations.

© 2022 American Pharmacists Association. Published by Elsevier Inc. All rights reserved.

#### Introduction

In recent years, there has been an increasing number of small molecule drug candidates with poor aqueous solubility and low oral bioavailability. Amorphous forms of such drugs have drawn considerable interest because of their solubility advantage. 1.2 However, pure amorphous drug is thermodynamically unstable and tends to convert to the more stable crystalline counterpart. 3 Amorphous solid dispersions (ASDs), formulated by molecularly dispersing an amorphous drug with a polymer, are used to improve physical stability. 4-6

Although no first principles model exists to predict the enhanced physical stability of ASDs, several viewpoints have been expressed: (1) polymeric matrices sterically hinder and impede crystallization of amorphous drugs and disrupt self-association of drug aggregates<sup>7</sup>; (2) incorporating a polymer with a higher glass transition temperature ( $T_g$ ) than that of the amorphous drug raises the  $T_g$  of an ASD, reducing molecular mobility<sup>3,8</sup>; and (3) drug/polymer combinations with relatively strong intermolecular interactions provide a route to physical stabilization.<sup>7,9</sup> In all of these viewpoints, it is assumed that

E-mail address: siege017@umn.edu (R.A. Siegel).

drug and polymer are dispersed homogenously at the molecular level, i.e. they are miscible. <sup>10</sup>

In the ASD literature, a miscible ASD is taken to consist of a single homogeneous phase with physical properties distinct from those of pure components. With this definition, an ASD consisting of a dilute dispersion of disconnected polymer chains in a "sea" of drug would be considered to be "immiscible." The miscibility limit is then the highest drug concentration above which an ASD is divided into a polymer rich domain and a pure amorphous drug domain.

(Before proceeding, we note that the ASD literature definition of miscibility is somewhat different from that used in physical chemistry. In the latter case, a miscible binary system is defined as "as stable homogeneous mixture which exhibits macroscopic features of a single-phase material." A dilute solid dispersion (low polymer concentration) would be considered to be miscible under this definition. We shall adhere to the ASD literature definition of miscibility in the present work.)

Since it is widely suggested that miscibility is an important indicator of stability against crystallization when a drug is formulated as an ASD, many experimental techniques have been applied to investigate it by identifying heterogeneous domains when the critical drug concentration is exceeded.  $^{13-15}$  One technique relies on determining the number of glass transition events. However, multiple glass transition events may be obscured when drug and polymer have similar  $T_{\rm g}$ 

<sup>\*</sup> Corresponding author at: Department of Pharmaceutics, University of Minnesota, Minneapolis, MN 55455, United States.

values, when domain sizes are very small (less than 20–30 nm), or when remixing takes place during heating. <sup>16</sup> Other methods applied to evaluate miscibility of ASDs include spectroscopic techniques, including Raman, <sup>16</sup> solid-state nuclear magnetic resonance (ssNMR), <sup>17</sup> Fourier-transform infrared (FTIR), <sup>18</sup> and fluorescence <sup>19</sup>; imaging techniques, including polarized light microscopy (PLM), <sup>20</sup> fluorescence microscopy, <sup>19</sup> scanning electron microscopy, <sup>21</sup> transmission electron microscopy, <sup>18,22</sup> and atomic force microscopy <sup>23</sup>; and their combinations. Although useful, these techniques can only provide qualitative information regarding drug-polymer miscibility and they are not universally applicable or accessible for routine use. <sup>15</sup>

Complementing the experimental techniques, the most popular theoretical scheme for determining miscibility is the Flory-Huggins theory, which is based on the mean field assumption.  $^{24-27}$  In this theory, the free energy of mixing per lattice site,  $F_{mix}$ , is given by

$$\frac{F_{\text{mix}}}{k_BT} = \frac{\phi}{N} ln\phi + (1-\phi) ln(1-\phi) + \chi\phi(1-\phi) \tag{1} \label{eq:finite}$$

where  $k_B$  is Boltzmann's constant, T is absolute temperature,  $\phi$  is the volume fraction of polymer, N is the ratio of molar volume of the polymer to that of the drug, and  $\chi$  is the Flory-Huggins interaction parameter. In this model, polymer acts as a solvent for the drug, and the miscibility limit is identified with the amorphous solubility of drug in polymer. The drug loading corresponding to the miscibility limit can be estimated by the intersection of the  $T_g$  curve and the spinodal curve,  $T_g$  which is obtained by taking the second derivative of Eq. (1) with respect to  $\phi$ , if  $\chi$  is inferred from the following:

$$\left(\frac{1}{T_{\rm m}^{\rm mix}} - \frac{1}{T_{\rm m}^{\rm pure}}\right) = \frac{-R}{\Delta H_{\rm fus}} \left[ \ln(1-\phi) + \left(1 - \frac{1}{N}\right)\phi + \chi\phi^2 \right] \eqno(2)$$

where  $T_m^{mix}$  is the melting temperature of crystalline drug/polymer dispersions,  $T_m^{pure}$  is the melting temperature of the pure drug, R is the gas constant, and  $\Delta H_{\rm fus}$  is the heat of fusion of crystalline drug.<sup>26</sup>

The accuracy of investigating miscibility of ASDs using Flory-Huggins theory is limited by three problems: (1) Flory-Huggins theory assumes that the drug/polymer solution is at equilibrium, but this only holds when temperature is above  $T_{\rm g}$  of the ASD. Hence, miscibility below  $T_{\rm g}$  can be predicted only by extrapolation or modeling<sup>10</sup>; (2) practically, different experimental conditions, including uniformity, particle size of drug/polymer crystalline dispersions, and different DSC heating rates, may lead to significantly different inferred  $\chi$  values<sup>28</sup>; and (3) Flory-Huggins theory assumes a mean field, with uniform  $\phi$ . This stipulation does not hold in a dilute solution of polymer in drug, since each polymer chain consists of contiguous monomers occupying sites in the same neighborhood, and regions between these locales are vacant of polymer.<sup>29</sup> This is reflected in the second term on the right-hand side of Eq. (3) obtained by expanding Eq. (1) at small  $\phi$ ,

$$\frac{F_{mix}}{k_B T} = \frac{\phi}{N} \ln \phi + \frac{1}{2} \phi^2 (1 - 2\chi) + \frac{1}{6} \phi^3 + O(\phi)$$
 (3)

where the monomer-monomer interaction  $\phi^2$  means  $\langle \phi^2 \rangle$ , rather than  $\langle \phi \rangle^2$ . Note that linear terms in  $\phi$  are ignored for simplicity. Therefore, the Flory-Huggins theory is best applied when polymer concentration is sufficiently high, and fluctuations can be neglected. To accurately describe miscibility of an ASD with a low polymer concentration (high drug loading), a method based on a different theory is needed.

Here we propose a rheology based method of miscibility determination of ASDs guided by the concept of the overlap concentration,  $c^*$ , is the concentration of a polymer solution for which the concentration of monomers inside a polymer coil is the same as the macroscopic average concentration, which was introduced by de Gennes and others in the 1970s. $^{30.33}$  We consider the small molecule drug, not the polymer, to be the solvent. $^{34}$  When the polymer concentration is sufficiently low, polymer coils are separated from each other leading

to polymer-rich and pure amorphous drug domains. When the polymer concentration exceeds  $c^*$ , polymer coils overlap and interpenetrate, the polymer in drug solution becomes semidilute/concentrated, and it can be regarded as a single homogeneous phase at the molecular level. Hence,  $c^*$  of polymer in an ASD is treated as the polymer loading corresponding to a pseudo-phase boundary.

The concentration  $c^*$  can be estimated as the point (actually a narrow range) where there is an abrupt change in slope of the viscosity-composition diagram when the drug/polymer mixture (ASD) is in the molten state. Importantly,  $c^*$  is also a threshold, below which ASDs, when quenched to ambient conditions, will be physically unstable, while above  $c^*$  the polymer will stabilize the amorphous drug against crystallization for long periods of time. In the present work, we demonstrate these principles using two poorly water-soluble model drugs, celecoxib (CEL) and loratadine (LOR), and four different grades (molecular weights) of polyvinylpyrrolidone (PVP).

In a recent publication we estimated  $c^*$  as the reciprocal of the intrinsic viscosity of the molten ASD system. <sup>34</sup> While the latter estimation was shown to be useful for the drug/polymer systems that were studied, we believe the present method to be more general. We also show here, for the first time, that ASDs formulated with polymer concentrations exceeding  $c^*$  retain their physical stability over long time periods at ambient conditions.

#### **Materials and Methods**

Materials

Celecoxib (CEL; Aarti Drugs Pvt Ltd., Mumbai, India), loratadine (LOR; Wuhan Biocar Bio-pharm Co. Ltd., Wuhan, China), polyvinyl-pyrrolidone (PVP; Kollidon® K12, K17, K25, and K30; BASF, Ludwigshafen, Germany), ethanol (EtOH; VWR International LLC., Radnor, PA), dichloromethane (DCM; Sigma-Aldrich, St. Louis, MO) and DMSO- $d_6$  (D, 99.9%; Cambridge Isotope Laboratories, Inc, Andover, MA) were used as received. Chemical structures of polymer and drugs are shown in Scheme 1.

# Methods

Preparation of Pure Amorphous CEL, LOR, and ASDs of CEL/PVP and LOR/PVP  $\,$ 

Pure amorphous CEL and LOR were prepared by heating  $\sim$ 20 mg of as-received crystalline powders at 165 °C (4.2 °C above melting temperature,  $T_{\rm m}$ ) and 145 °C (10.7 °C above  $T_{\rm m}$ ), respectively, for

CF<sub>3</sub>

Celecoxib (CEL)

$$T_g = 57.5 \, ^{\circ}\text{C}$$
 $T_m = 160.8 \, ^{\circ}\text{C}$ 

Density: 1.40 g/cm<sup>3</sup>

Polyvinylpyrrolidone (PVP)

CI

Loratadine (LOR)

 $T_g = 35.6 \, ^{\circ}\text{C}$ 
 $T_m = 134.3 \, ^{\circ}\text{C}$ 

Density: 1.24 g/cm<sup>3</sup>

Scheme 1. Molecular structures of CEL, LOR, and PVP.

 $\sim$ 3 min using a hot plate (Model #HS40; Torrey Pines Scientific, Carlsbad, CA) to ensure complete melting. Drug melts were quenched using liquid nitrogen.

CEL and LOR ASDs with PVP at different polymer loadings were prepared by melting and quenching 500 mg of spray dried drug/polymer mixtures under conditions identical to those for preparing the corresponding pure amorphous drugs. Meltquenched samples were ground manually using a mortar and pestle to reduce particle size, and then sieved. Particles of size 250–300  $\mu$ m were used for physical stability testing. All samples were confirmed to be devoid of crystallinity by XRPD, PLM, and DSC (Figures S1-S6).

#### Differential Scanning Calorimetry (DSC)

Powders (3–6 mg) were loaded into Tzero aluminum pans with pin holes. Samples were first heated from 0 °C to 170 °C (CEL ASDs) or 145 °C (LOR ASDs) at 10 °C/min to erase thermal history, quenched to 0 °C, held isothermally for 5 min, and reheated at 10 °C/min to the original high temperature in a differential scanning calorimeter (Q1000; TA Instruments, New Castle, DE) under continuous helium purge at a flow rate of 25 mL/min.

#### Size Exclusion Chromatography (SEC)

Number  $(M_{\rm n})$  and weight  $(M_{\rm w})$  average molecular weights and dispersities (D) of PVPs of different grades were determined by SEC (Agilent 1200 Series; Agilent, Santa Barbara, CA) equipped with two Viscotek I-series columns (MBMMW-3078), a Wyatt Dawn Heleos II multiangle light scattering detector, and a Wyatt Optilab T-rEX differential refractometer (Wyatt Technology, Santa Barbara, CA), with flow rate 1.0 mL/min. Briefly, a  $\sim$ 5 mg/mL solution of each PVP sample was prepared using DMF containing 0.05 M LiBr, and passed through a PTFE 0.22  $\mu$ m syringe filter to remove dust. Elution cures are presented in Figure S7.

# Rheometry

Zero-shear-rate viscosity ( $\eta$ ) of pure drug and drug/polymer melts was measured using a rheometer (ARES; TA Instruments, New Castle, DE). A parallel plate geometry with diameter 25 mm was employed. Briefly, ~800 mg of ASD powder was placed on the bottom plate after zero torque, normal force, and gap calibrations. The gap between the parallel plates was fixed at 1 mm (corrected for thermal expansion of the plates). CEL and LOR ASD powders were melted at 165 °C and 145 °C, respectively, and equilibrated for ~5 min to guarantee complete melting before each measurement. A steady rate sweep test was performed with the initial rate of 1 s<sup>-1</sup> and the final rate of 100 s<sup>-1</sup> with continuous nitrogen purge at a flow rate of 3 standard cubic feet per minute (SCFM).

# *X-ray Powder Diffraction (XRPD)*

X-ray powder diffractograms of CEL/PVP (held at 70 °C) and LOR/PVP ASDs (held at 60 °C) were obtained using an X-ray diffractometer (X'pert Pro; PANalytical, Westborough, MA) with Cu  $K\alpha$  radiation ( $\lambda$  = 1.540598 Å). Samples were scanned between  $2\theta$  = 5–35° with step size 0.016° at 1 s/step. Tube voltage and amperage were set as 45 kV and 40 mA, respectively.

#### *Variable Temperature X-ray Powder Diffraction (VTXRD)*

CEL/PVP and LOR/PVP ASDs with 5, 10, 20, and 30% polymer loadings were evaluated using an X-ray diffractometer (D8 Advance; Bruker AXS, Madison, WI) equipped with a variable temperature stage (TTK 450; Anton Paar, Graz-Straßgang, Austria), and a Si strip one-dimensional detector (LynxEye; Bruker AXS, Madison, WI). Measurements were performed in 10 °C increments from 25 °C up to 115 °C. Co  $K_{\alpha}$  radiation (( $\lambda$  = 1.78899 Å, 35 kV, and 45 mA) was used,

and data were collected in the range  $2\theta$  = 5–35° with step size 0.019699° at 0.5 s/step. The duration of each measurement was approximately 12 min.

#### **Results and Discussion**

To successfully determine  $c^*$  (the miscibility limit) from the viscosity-composition diagram, two prerequisites must be met. First, both drug and polymer should be chemically stable at the processing temperature (above  $T_{\rm m}$  of the drug). Second, the drug must serve as a good or a theta solvent for the polymer. The latter condition is essential to avoid potential liquid-liquid phase separation.<sup>35</sup>

#### Chemical Stability

<sup>1</sup>H NMR spectra of melt-quenched CEL and LOR and those of corresponding as-received powders are identical (Figure S8), confirming chemical stability of CEL and LOR during melt quenching.

Interaction Between Drug and Polymer: Melting Point Depression

Traditionally in the pharmaceutical literature, the polymer is considered as a solvent for the drug. 10 Here, the small molecule drug is considered a solvent for the polymer. Solvents for polymers are broadly divided into three categories, i.e., good, theta, and poor.<sup>32</sup> For a theta solvent, intermolecular interactions (including all types of attractive interactions, such as van der Waals forces, hydrogen bonding, and ionic interactions) are rather unfavorable, so that chains behave ideally with respect to their conformations, and adopt a random walk, with a radius of gyration (the root-mean-square, massweighted distance of monomers from its center of mass),  $R_g$ , such that  $R_{\rm g} \sim M^{0.5}$ . For a good solvent, pairwise intermolecular interactions between a monomer and a solvent molecule are stronger than that in the theta condition. In this case, a polymer coil of molecular weight, M, swells to attain  $R_g \sim M^{0.59}$ . In a poor solvent, interactions between polymer and solvent are weaker than in the theta condition, which may lead to phase separation into polymer-rich and polymerlean domains. 32,37 It should be noted, however, that rather large values of M may be necessary to distinguish between good and theta solvent behaviors.37

Melting point depression of CEL [164.9 °C (5%), 164.0 °C (10%), 163.3 °C (20%), and 162.4 °C (30%)] and LOR [135.7 °C (5%), 134.6 °C (10%), 133.1 °C (20%), 132.3 °C (30%)] crystals by PVP (Fig. 1a and 1b, respectively) provides evidence pointing to favorable interactions between the two model drugs and PVP.<sup>38</sup> At equilibrium, if a drug melt is compatible with a polymer, the chemical potential of the drug in the mixture is lower than that of the pure molten drug. Consequently, a lower melting temperature is observed.<sup>28</sup> Since melting endotherms of CEL are broad, due to polymorph cross-nucleation induced by heating (Tms (onset) of CEL are 160.8 and 163.5 °C, for Form III and Form I, respectively),  $^{39}$  endpoints ( $T_{end}$ , identified from the intersection of the falling edge of the melting endotherm and the post melting baseline<sup>40</sup>), instead of onset of melting endotherms, were used to delineate the trend of melting point depression of drug crystal in the presence of PVP additive. Although  $T_{\rm end}$  is more sensitive to heating rate compared with the onset, practically, heating rates were consistent for all samples. Therefore,  $T_{end}$  can give the same rank order as the onset temperature. These observations indicate that of CEL and LOR are good solvents for PVP at high temperatures, although no significant hydrogen bonding was observed from the FTIR spectra for both CEL/PVP and LOR/PVP ASDs (Figs. S9 and S10).

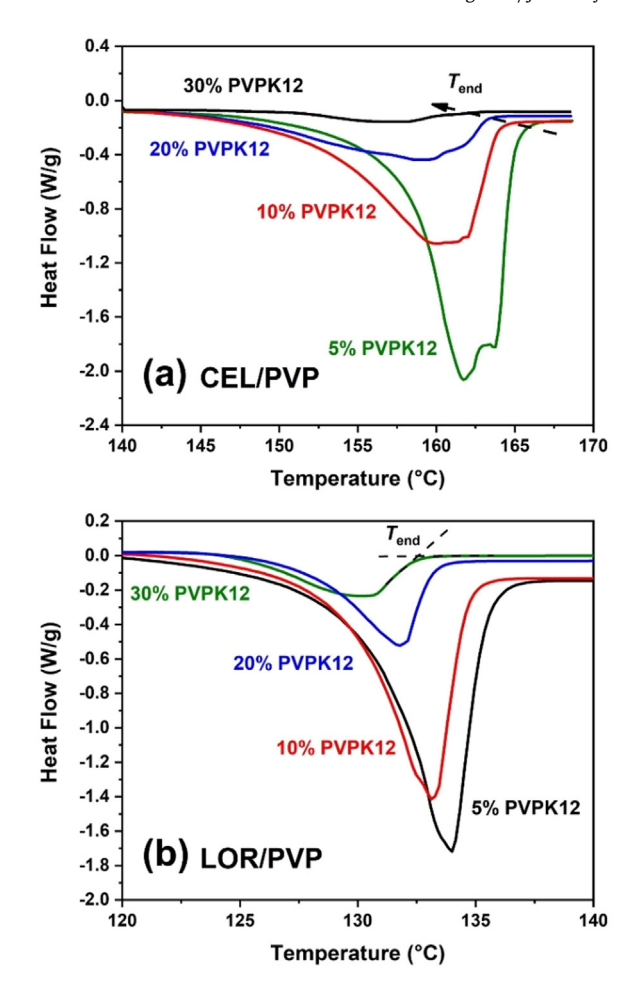


**Figure 1.** (a) Melting endotherms of (a) CEL and (b) LOR crystals in the presence of 5%, 10%. 20%, and 30% PVP K12.

Miscibility Determination by Rheological Analysis

Miscibility Determination by the Viscosity-Composition Diagram

Roughly, three regimes, namely dilute, semidilute, and concentrated, are observed when the polymer is in a good solvent.<sup>35</sup> In the dilute regime, polymer coils are situated apart from each other, therefore, intermolecular interactions between adjacent polymer coils are negligible (Fig. 2, left). Consequently, the viscosity of a dilute polymer solution is an approximately linear function of polymer concentration:

$$\eta = \eta_s (1 + c[\eta]_w) \tag{4}$$

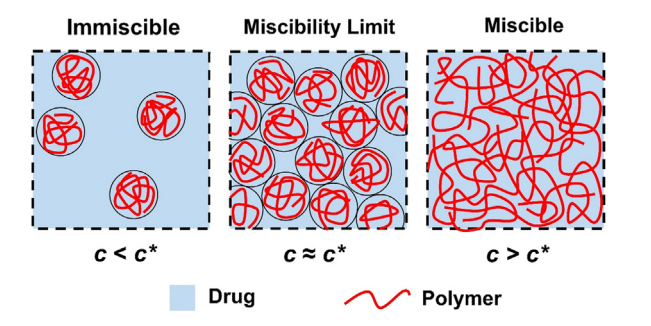


**Figure 2.** Scheme of the crossover between dilute (left) and semidilute/concentrated (right) polymer solutions. The light blue background indicates a drug melt serving as a solvent, and red coils indicate polymers dissolved in a drug melt. (For interpretation of the references to color in this figure legend, the reader is referred to the web version of this article.)

where  $\eta$  is the viscosity of the polymer solution (molten ASD),  $\eta_s$  is the viscosity of the pure solvent (drug melt), and c is the polymer concentration (w/w,%). The term,  $[\eta]_w$  in Eq. (4) is the intrinsic viscosity of the drug/polymer combination, expressed in units of  $\%^{-1}$ . It differs from the conventional intrinsic viscosity,  $[\eta]$ , in that the latter is calculated based on w/v polymer concentrations and is expressed as cm³/g.

In the semidilute regime, polymer coils start to overlap (Fig. 2, middle), and coil-coil interactions lead to a change in the slope of the viscosity-concentration curve. The crossover between dilute and semidilute regimes occurs at the overlap concentration,  $c^*$  (Fig. 2, middle).<sup>30,35</sup>

In the concentrated regime, the viscosity of a concentrated polymer solution increases more steeply well above  $c^*$ , roughly in proportion to  $c^{4-5}$ . This is partially due to entanglement effects (topological interactions), which are more significant for polymers with high molecular weights,  $^{35}$  but it can also reflect an increasing glass transition temperature (and therefore slower segmental dynamics).

The overlap concentration  $c^*$  can be correlated with the miscibility limit of ASDs. Miscibility is defined here as intimate mixing of the amorphous drug and polymer at the molecular level, forming a single homogeneous domain.  $^{26,41}$  A dilute ASD, with polymer concentration below  $c^*$ , consists of two kinds of domains: one is a drug/polymer molecular mixture within each coil, and the other consists of pure drug and is devoid of polymer (Fig. 2, left). As polymer concentration increases, the former kind of domain becomes more prevalent, and the latter diminishes. When the polymer concentration is above  $c^*$ , coils are closely packed or entangled. Such an ASD can be considered homogeneously mixed as a single domain (Fig. 2, right). Therefore, we propose that  $c^*$  can be assigned as the polymer loading corresponding to the miscibility limit of ASDs.

The value of  $c^*$  can be determined as the location of a sharp change in slope of the viscosity-composition diagram in the melt. For CEL/PVP ASDs,  $c^*$  values for PVP K12 ( $M_w \sim 4$  K), PVP K17 ( $M_w \sim 8$  K), PVP K25 ( $M_{\rm w}$  ~50 K), and PVP K30 ( $M_{\rm w}$  ~55 K) are approximately 12%, 10%, 5%, and 4% polymer concentration, respectively (Fig. 3a). Similarly, for LOR/PVP ASDs, c\* values for PVP K12, PVP K17, PVP K25, and PVP K30 are around 15%, 10%, 5%, and 4% polymer concentration, respectively (Fig. 3b). It should be recognized that this change in slope is not immediate, and that  $c^*$  corresponds to a (albeit narrow) range of polymer concentrations. The location of this "c\* range" shifts downward with increasing polymer molecular weight, as shown in Fig. 3a and 3b for CEL/PVP and LOR/PVP combinations, respectively. This observation is in line with the de Gennes theory of the transition between dilute and semidilute polymer solutions, since a single polymer chain with a larger molecular weight can pervade a larger volume. Therefore, a smaller fraction of polymer (smaller  $c^*$ ) is needed to fill in the space.<sup>30</sup> It is also consistent with the trend previously reported for indomethacin/PVP and felodipine/PVP systems.<sup>34</sup>

Comparison of c\* Determination by the Viscosity-Composition Diagram with the Inverse of  $[\eta]$ 

Another correlation used to estimate  $c^*$  is  $c^* \cong 1/[\eta]_w$ .  $^{34}$  It comes from an estimation that, when polymer coils start to densely pack, they contribute as much to the overall viscosity as does the pure solvent. This is obtained by equating the first and second terms on the right-hand side in Eq. (4), which represent the contributions to the solution viscosity from the pure solvent and isolated coils, respectively. However, this estimation is rough, and other estimations such as  $c^* \cong 2/[\eta]_w$  or  $c^* \cong 2.5/[\eta]_w$  have been proposed. No method is optimal from a theoretical standpoint since there is no consensus on the theory of  $c^*$ . Here,  $c^*$  of CEL/PVP and LOR/PVP systems determined from the viscosity-composition diagram and from  $[\eta]_w^{-1}$ , with the coefficient between 1 and 2.5, are given in Table 1 for comparison. For LOR/PVP ASDs, results are comparable since the contribution of

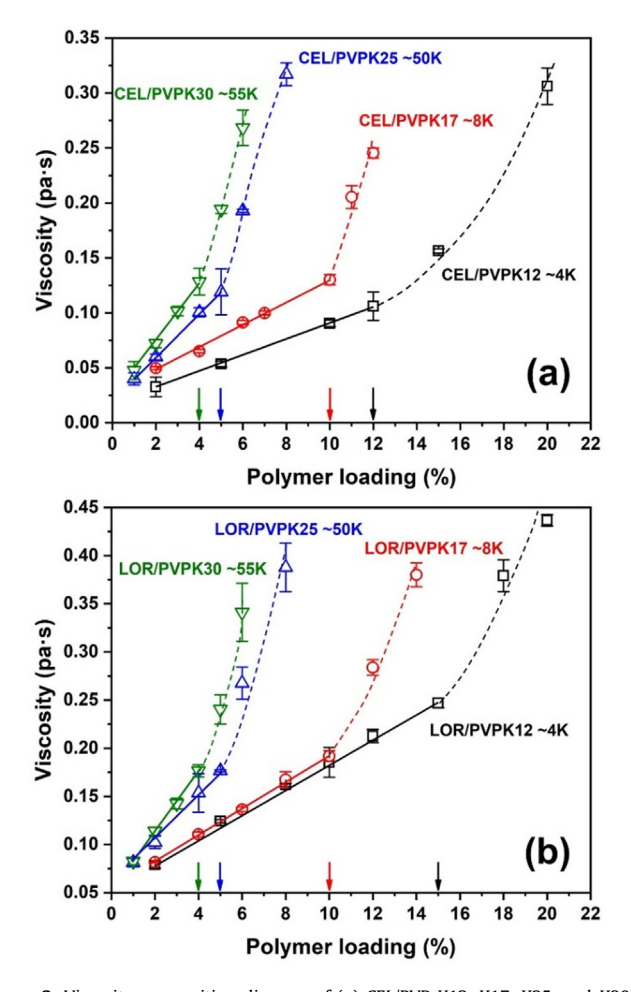


**Figure 3.** Viscosity-composition diagram of (a) CEL/PVP K12, K17, K25, and K30 at 165 °C and (b) LOR/PVP K12, K17, K25, and K30 at 145 °C. Each viscosity data point was the average value for 3–5 measurements of at least three independent prepared samples. Arrows correspond to  $c^*$ , where there is a break in the slopes of the individual viscosity-concentration curves.

overall viscosity from PVP is roughly two times greater than that of the pure LOR melt at the crossovers (Fig. 3b). However,  $c^*$  determined by viscosity-composition diagrams are slightly greater than the latter method for CEL/PVP combinations, since PVP contributes approximately four times more to the viscosity than the pure CEL (Fig. 3a). In the following sections,  $c^*$  values of CEL/PVP and LOR/PVP were estimated from corresponding viscosity-composition diagrams.

#### Physical Stability Against Crystallization

For ASDs, it is widely recognized that miscibility is a significant indicator of physical stability, since an amorphous drug in an immiscible dispersion is anticipated to crystallize more rapidly, due to the less effective nucleation and crystal growth inhibition by an inadequate polymer concentration below the miscibility limit. <sup>19,41</sup> To verify the hypothesis that  $c^*$  is the critical polymer concentration corresponding to the estimated miscibility limit, the crystallization tendency of ASDs with various polymer loadings was assessed by both XRPD and VTXRD. It is assumed that the glass inherits the structure of its precursor liquid, i.e., the conformation of a polymer in a drug melt is trapped in the glassy state, and therefore that  $c^*$  is the same in the glassy state as in the melt.

Fig. 4 provides a comparison of crystallization tendencies of CEL/ PVP ASDs with four different polymer loadings using XRD by both the variable temperature and the isothermal method. For the variable temperature study, for ASDs containing 5% and 10% polymer, which were below  $c^*$ , the onset of crystallization of CEL was at 95 °C ( $T_g$ <sub>CEL</sub> + 37.5 °C) (Fig. 4a). The characteristic peaks indicate that both Form III and Form I appeared.<sup>39</sup> This is due to polymorph cross-nucleation, i.e., when temperature is above 90 °C, Form III seeds could either grow or cross-nucleate Form I, assuming PVP has no influence on the nucleation process of CEL.<sup>39</sup> When the polymer loading was slightly above  $c^*$  ( $\sim$ 12%), i.e., 20% polymer loading, crystallization commenced at 115 °C ( $T_{\rm g,CEL}$  + 57.5 °C), which was 20 °C higher than for the 5% and 10% polymer samples (Fig. 4b). It is worth noting that the tiny amount of crystallization for 20% polymer loaded ASD at 115 °C could partially be ascribed to the hygroscopicity of PVP, since samples were stored overnight under ambient conditions (23 °C and  $\sim$ 50% RH) and scanned at  $\sim$ 60% RH. Moisture absorption may have led to a ternary drug/polymer/water system with enhanced crystallization tendency. 11,42 When polymer loading was further increased to 30%, no crystallization was observed at the end of the study at 115 °C, even under a relatively high humidity environment.

For the isothermal accelerated physical stability study at 70 °C and 0% RH, the same significant difference of CEL/PVP ASD below and above its  $c^*$  has been demonstrated. For ASDs containing 5% and 10% polymer, which were below  $c^*$ , the first evidence of crystallization of CEL appeared promptly by the third and fifth day, respectively (Fig. 4c). However, when the PVP concentration exceeded  $c^*$  (concentrations 20% and 30%), no characteristic peaks of CEL crystal were observed by the end the entire study (18 days) (Fig. 4d).

Fig. 5 shows both variable temperature and isothermal crystallization tendencies of LOR/PVP ASDs with polymer loadings below and above  $c^*$  under a certain temperature elevation program and the storage condition of 60 °C and 0% RH. At polymer loadings of 5% and 10%.

**Table 1**  $M_{\rm n}$ ,  $M_{\rm w}$ , and D of PVPK12, K17, K25, and K30. Comparison of  $c^*$  of PVP in CEL and LOR determined by methods following Viscosity-composition diagram and  $[\eta]^{-1}$  (coefficient between 1 and 2.5).

	$M_{\rm n}$	$M_{ m w}$	Đ	$c^*$ in CEL by Viscosity –	$c^*$ in CEL by	c* in LOR by Viscosity –	$c^*$ in LOR by
	(g/mol)	(g/mol)	$(M_{\rm w}/M_{\rm n})$	composition diagram (%)	$[\eta]_{w^{-1}}(\%)$	composition diagram (%)	$[\eta]_{\mathrm{w}^{-1}}(\%)$
PVPK12	2,300	3,790	1.65	~12	3.2-8.1	~15	8.2-20.4
PVPK17	4,050	7,340	1.81	~10	2.7-6.7	~10	4.0-10.0
PVPK25	25,710	49,480	1.92	~5	1.2-3.0	~5	2.3-5.8
PVPK30	30,360	55,090	1.81	~4	0.7-1.8	~4	1.8-4.5

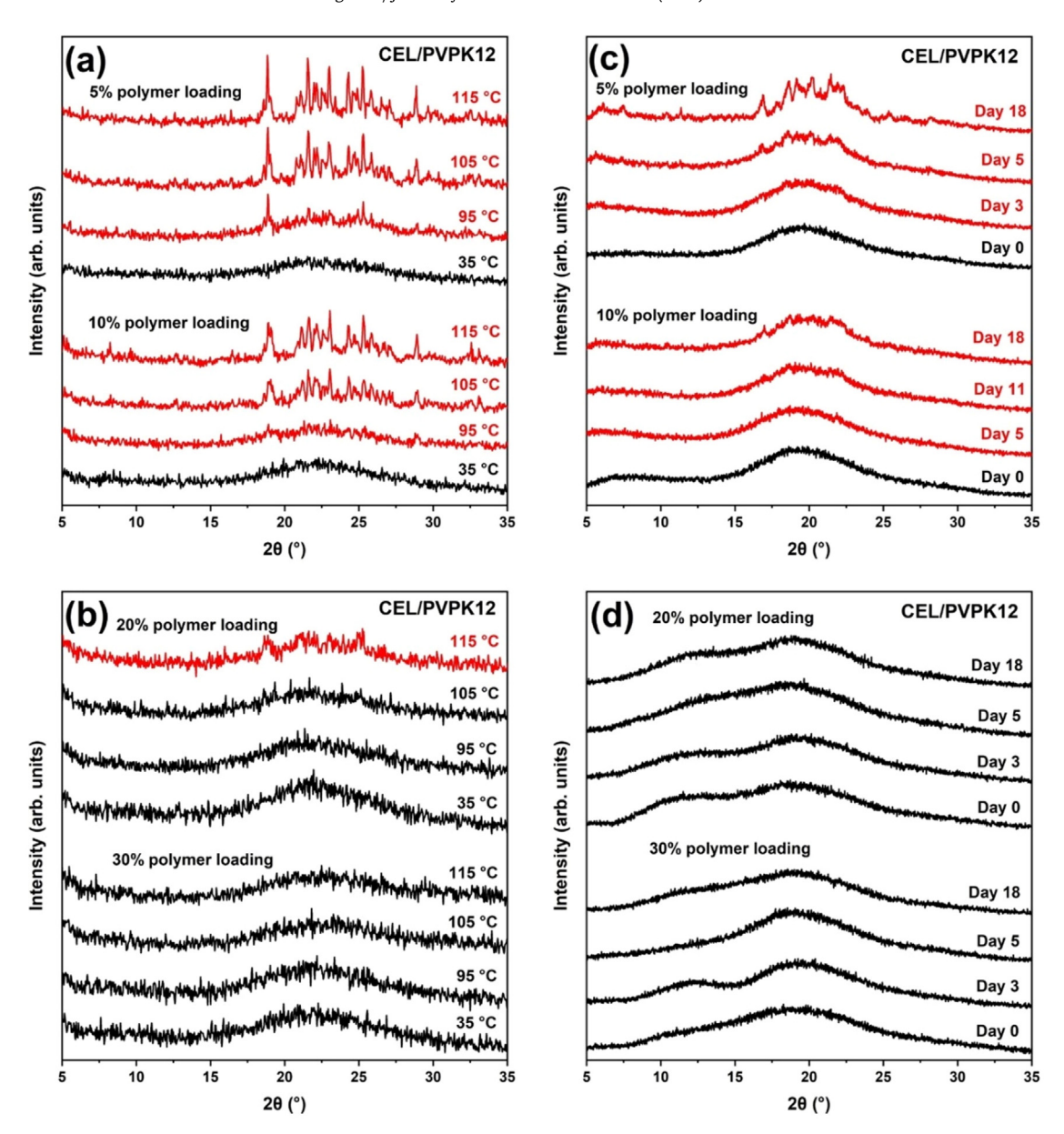


**Figure 4.** X-ray diffraction patterns of CEL/PVP K12 ASD with various polymer loadings (a) 5% and 10% polymer loading (below  $c^*$ ), (b) 20% and 30% polymer loading (above  $c^*$ ) subjected to a controlled temperature program under  $\sim$ 60% relative humidity (RH). The temperatures at which the powder patterns were obtained are indicated. (c) 5% and 10% polymer loading (below  $c^*$ ), (d) 20% and 30% polymer loading (above  $c^*$ ) at day zero and after specified days stored at 70 °C and 0% RH. The days at which the powder patterns were obtained are indicated. CEL crystallization is evident from the appearance of their characteristic peaks, which are marked in red. (For interpretation of the references to color in this figure legend, the reader is referred to the web version of this article.)

which are below  $c^*$  ( $\sim$ 15%), amorphous LOR showed first evidence of crystallization rapidly at 85 °C ( $\sim$ 50 °C higher than the  $T_{\rm g}$  of LOR) and by day 2 (Fig. 5a and 5c). Characteristic peaks indicate that only Form I was present. Significantly reduced crystallization propensity was observed when the polymer loading was slightly above  $c^*$ . For 20% polymer-loaded LOR/PVP ASD, crystallization occurred at 105 °C (20 °C higher than for 5% and 10% LOR ASDs) and after ten days, while 30% polymer loading inhibited LOR crystallization completely for the duration of studies at 115 °C and two weeks, for variable temperature and isothermal stability studies, respectively (Fig. 5b and 5d).

The above accelerated physical stability studies were carried out in the supercooled liquid state. However, formulation scientists are more interested in the long-term stability in the glassy state. Fig. 6 shows the crystallization tendency of CEL/PVP K12 ASDs stored under ambient conditions for one year. For 20% and 30% polymer loading samples (above  $c^*$ ), no characteristic peaks can be observed. In

contrast, samples below  $c^*$  (5% and 10% polymer loading ASDs) crystallized significantly. These results suggest that the  $c^*$  determined from the viscosity-composition diagram is a reliable predictor of physical stability against crystallization of an ASD.

# Procedure for Miscibility Determination of ASD

To facilitate adoption of the method presented in this work, a procedure for miscibility determination is shown in Scheme 2. In the first step, chemical stability of drug and polymer are verified at a chosen processing temperature, typically 5–10 °C above the melting temperature of the drug, where one can expect a complete and uniform drug/polymer melt for the accuracy of viscosity measurement. NMR, HPLC, and mass spectrometry are good techniques for detecting drug thermal degradation. <sup>43</sup>

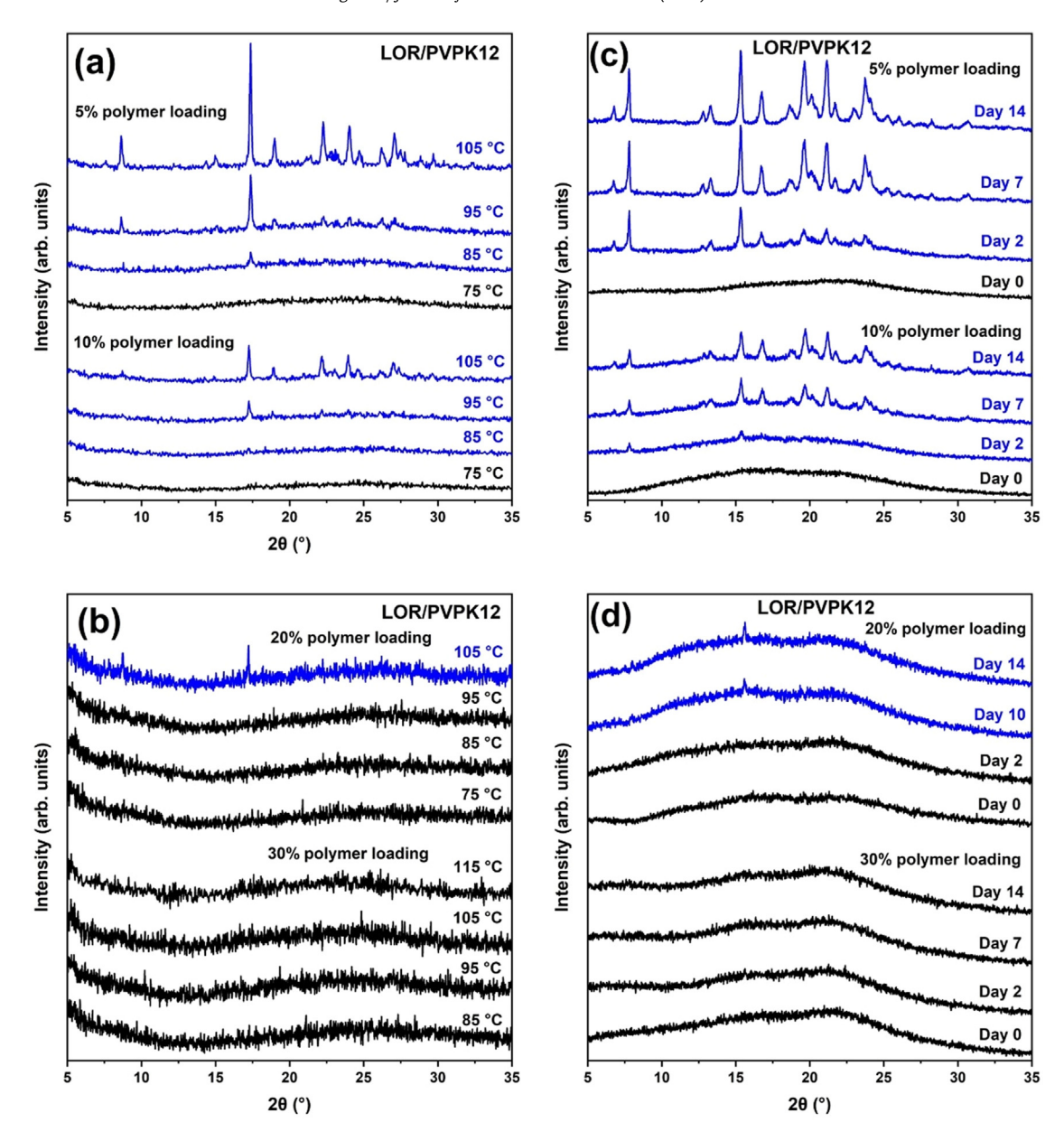


**Figure 5.** X-ray diffraction patterns of LOR/PVP K12 ASD with various polymer loadings (a) 5% and 10% polymer loading (below  $c^*$ ), (b) 20% and 30% polymer loading (above  $c^*$ ) subjected to a controlled temperature program under  $\sim$ 20% RH. The temperatures at which the powder patterns were obtained are indicated. (c) 5% and 10% polymer loading (below  $c^*$ ), (d) 20% and 30% polymer loading (above  $c^*$ ) at day zero and after specified days stored at 60 °C and 0% RH. The days at which the powder patterns were obtained are indicated. LOR crystallization is evident from the appearance of their characteristic peaks, which are marked in blue. (For interpretation of the references to color in this figure legend, the reader is referred to the web version of this article.)

Second, to avoid phase separation during viscosity measurement, a drug that serves as a good or theta solvent for the polymer is required. Phase separation, which is indicative of poor solvency, can sometimes be observed optically if domains are large enough. Also, when the molten drug is a good solvent for the polymer, the melting point of the drug crystal is reduced monotonically with increasing polymer concentration. <sup>40</sup> The route of drug/polymer mixture preparation, which affects uniformity of crystalline dispersions, can influence the accuracy of  $T_{\rm end}$  significantly. For example, Tao et al. showed that a poorly mixed sample prepared by hand or ball milling gives a higher  $T_{\rm end}$  than a well-mixed sample prepared by a cryogenic milling. <sup>40</sup>

The third and the most critical step is to measure the viscosity of the drug/polymer melt at various polymer concentrations. To obtain consistent data, the processing temperature should be kept constant for all measurements since viscosity is temperature dependent. To be sure that the measured viscosity data is reliable, one can extrapolate the linear region of the viscosity-composition diagram, following Eq. (4), to zero polymer concentration, and verify that the extrapolated value equals the measured viscosity of the neat drug melt at the same temperature. For example, the extrapolated viscosities of LOR melts with PVP K12, K17, K25, and K30 (Fig. 3b), 0.0571 pa\*s, 0.0544 pa\*s, 0.0559 pa\*s, and 0.0512 pa\*s, respectively, are very close to the measured viscosity of pure LOR melt, 0.0557 pa\*s. This provides confidence in the accuracy of the linear fitting used for determining  $c^*$ .

Finally, the crystallization tendency of ASDs with polymer loadings below and above  $c^*$  should be assessed to verify the accuracy of the prediction. The onset of crystallization can be identified with samples stored at various conditions using room temperature XRD, or VTXRD either by finding the onset temperature by heating with a

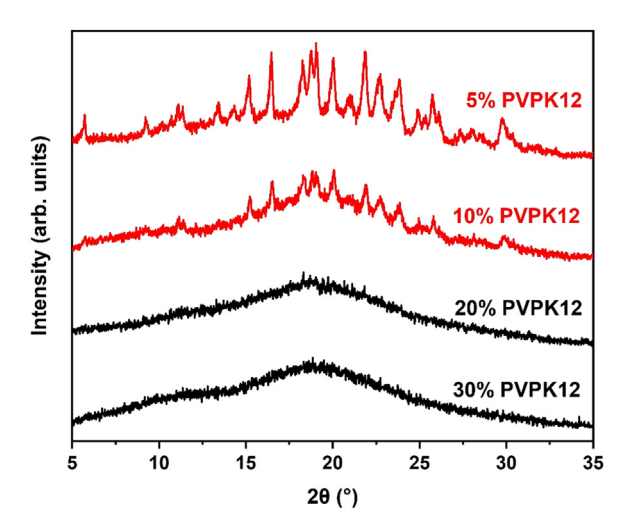
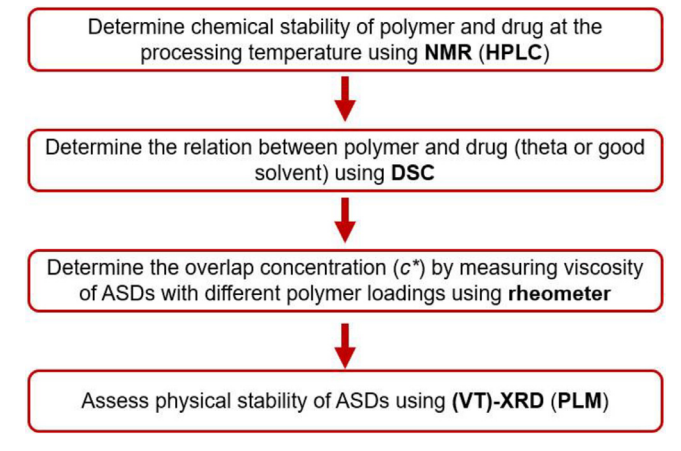


**Figure 6.** X-ray diffraction patterns of CEL/PVP K12 ASD with various polymer loadings 5%, 10% (below  $c^*$ ), 20%, and 30% (above  $c^*$ ) stored under ambient conditions for one year.

constant rate or detecting the onset time during isothermal crystallization at higher temperatures. Particle size distribution of ASD powders should be carefully controlled to minimize the impact of significantly different surface and bulk crystal growth rates on crystallization kinetics below  $T_{\rm g}$ . Alternatively, crystallization kinetics (surface and bulk) of ASDs in a film geometry prepared by rapid quench on a glass slide stored at certain conditions can be also monitored by polarized light microscopy. 45

Since the present model considers an ASD as a binary solution, i.e., a polymer dissolved in a drug, one of limitations of this methodology is that the moisture absorption is not considered. Amorphous-amorphous phase separation can be induced in a miscible ASD by high RH storage, especially for hygroscopic polymers such as PVP and PVP-VA. AG A generalized model for such ternary drug/polymer/water systems should be explored in future work. Also, we are not confident as to whether the miscibility of ASDs prepared by solvent mediated approaches, such as solvent evaporation or coprecipitation, can be well predicted by the current method, since solvent removal kinetics may influence polymer conformation in final products. A procedure for predicting physical stability of ASDs prepared by solvent mediated processes remains to be explored.



**Scheme 2.** Procedure of miscibility determination of ASDs.

#### **Conclusions**

In this work, correlation between  $c^*$  and miscibility of ASDs has been demonstrated. The value of  $c^*$  can be determined by measuring the viscosity of the drug/polymer melt with various polymer loadings and plotting the corresponding viscosity-composition diagram. When polymer loadings are below  $c^*$ , ASDs show strong tendency to crystallize, while ASDs with polymer loadings greater than  $c^*$  exhibit elevated physical stability. It is worth noting that  $c^*$  can be quite low for a good solvent system when the molecular weight is large. This indicates that the use of higher molecular weight polymers is more effective for preparing high drug loaded ASD formulation in terms of crystallization inhibition. However, for practical purposes, polymer loading selected for a formulation should be slightly greater than  $c^*$ to account for the effect of moisture, which is almost impossible to avoid during manufacturing and long term storage. Validating this miscibility determination procedure with more drug/polymer combinations and demonstrating its applicability to ASD formulation with high drug loading is a logical next step along this line of research.

### **Declaration of Competing Interest**

The authors have no competing financial interests or personal relationships to declare.

# Acknowledgments

S.S. thanks Prof. Masao Doi (Wenzhou Institute, UCAS) for delightful communication on  $c^*$  and Dr. David Giles (Polymer Characterization Facility, UMN) for helpful discussion of viscosity measurement. Parts of this work were carried out in the Polymer Characterization Facility and the Characterization Facility, UMN, which receives partial support from the NSF through the MRSEC (DMR-2011401) and the NNCI (ECCS-2025124) programs. Funding from Industrial Partners for Research in Interfacial and Materials Engineering (IPRIME, UMN) is also acknowledged.

# **Supplementary Materials**

Supplementary material associated with this article can be found in the online version at doi:10.1016/j.xphs.2022.08.028.

#### References

- Newman A, Knipp G, Zografi G. Assessing the performance of amorphous solid dispersions. J Pharm Sci. 2012;101(4):1355–1377.
- Jermain SV, Brough C, Williams RO. Amorphous solid dispersions and nanocrystal technologies for poorly water-soluble drug delivery – an update. Int J Pharm. 2018;535(1):379–392.
- 3. Yu L. Amorphous pharmaceutical solids: preparation, characterization and stabilization. *Adv Drug Deliv Rev.* 2001;48(1):27–42.
- Serajuddin ATM. Solid dispersion of poorly water-soluble drugs: early promises, subsequent problems, and recent breakthroughs. J Pharm Sci. 1999;88(10):1058– 1066.
- Chiou WL, Riegelman S. Pharmaceutical applications of solid dispersion systems. J Pharm Sci. 1971;60(9):1281–1302.
- Newman A, Zografi G. What are the important factors that influence API crystallization in miscible amorphous API—excipient mixtures during long-term storage in the glassy state? Mol Pharm. 2022;19(2):378–391.
- Taylor LS, Zografi G. Spectroscopic characterization of interactions between PVP and indomethacin in amorphous molecular dispersions. *Pharm Res.* 1997;14 (12):1691–1698.
- Hancock BC, Shamblin SL, Zografi G. Molecular mobility of amorphous pharmaceutical solids below their glass transition temperatures. *Pharm Res.* 1995;12(6):799–806.
- Kothari K, Ragoonanan V, Suryanarayanan R. The role of drug—polymer hydrogen bonding interactions on the molecular mobility and physical stability of nifedipine solid dispersions. Mol Pharm. 2015;12(1):162–170.
- Qian F, Huang J, Hussain MA. Drug—polymer solubility and miscibility: stability consideration and practical challenges in amorphous solid dispersion development. J Pharm Sci. 2010;99(7):2941–2947.

- 11. Newman A. Pharmaceutical Amorphous Solid Dispersions. Wiley; 2015.
- Olabisi O. Interpretations of polymer-polymer miscibility. J Chem Educ. 1981;58

   (11) 944
- Newman A, Munson E. Characterizing miscibility in amorphous solid dispersions. Am Pharm Rev. 2012;15:92–98.
- Meng F, Dave V, Chauhan H. Qualitative and quantitative methods to determine miscibility in amorphous drug—polymer systems. *Eur J Pharm Sci.* 2015;77:106–111.
   Thakore SD, Akhtar J, Jain R, Paudel A, Bansal AK. Analytical and computational
- Thakore SD, Akhtar J, Jain R, Paudel A, Bansal AK. Analytical and computational methods for the determination of drug-polymer solubility and miscibility. Mol Pharm. 2021;18(8):2835–2866.
- Qian F, Huang J, Zhu Q, et al. Is a distinctive single Tg a reliable indicator for the homogeneity of amorphous solid dispersion? Int J Pharm. 2010;395(1):232–235.
- Yuan X, Sperger D, Munson EJ. Investigating miscibility and molecular mobility of nifedipine-PVP amorphous solid dispersions using solid-state NMR spectroscopy. *Mol Pharm*. 2014;11(1):329–337.
- Li N, Taylor LS. Nanoscale infrared, thermal, and mechanical characterization of telaprevir-polymer miscibility in amorphous solid dispersions prepared by solvent evaporation. Mol Pharm. 2016;13(3):1123-1136.
- Tian B, Tang X, Taylor LS. Investigating the correlation between miscibility and physical stability of amorphous solid dispersions using fluorescence-based techniques. Mol Pharm. 2016;13(11):3988–4000.
- Parikh T, Gupta SS, Meena AK, Vitez I, Mahajan N, Serajuddin ATM. Application of film-casting technique to investigate drug—polymer miscibility in solid dispersion and hot-melt extrudate. J Pharm Sci. 2015;104(7):2142–2152.
- Karavas E, Georgarakis M, Docoslis A, Bikiaris D. Combining SEM, TEM, and micro-Raman techniques to differentiate between the amorphous molecular level dispersions and nanodispersions of a poorly water-soluble drug within a polymer matrix. *Int J Pharm*. 2007;340(1):76–83.
- Marsac PJ, Rumondor ACF, Nivens DE, Kestur US, Stanciu L, Taylor LS. Effect of temperature and moisture on the miscibility of amorphous dispersions of felodipine and poly(vinyl pyrrolidone). J Pharm Sci. 2010;99(1):169–185.
- Purohit HS, Taylor LS. Miscibility of itraconazole—hydroxypropyl methylcellulose blends: insights with high resolution analytical methodologies. *Mol Pharm*. 2015;12(12):4542–4553.
- 24. Flory PJ. Thermodynamics of high polymer solutions. J Chem Phys. 1942;10(1):51-61.
- Huggins ML. Theory of solutions of high polymers<sup>1</sup>. J Am Chem Soc. 1942;64 (7):1712–1719.
- Marsac PJ, Shamblin SL, Taylor LS. Theoretical and practical approaches for prediction of drug—polymer miscibility and solubility. *Pharm Res.* 2006;23(10):2417.
- Marsac PJ, Li T, Taylor LS. Estimation of drug—polymer miscibility and solubility in amorphous solid dispersions using experimentally determined interaction parameters. *Pharm Res.* 2008;26(1):139.

- Sun Y, Tao J, Zhang GGZ, Yu L. Solubilities of crystalline drugs in polymers: an improved analytical method and comparison of solubilities of indomethacin and nifedipine in PVP, PVP/VA, and PVAc. J Pharm Sci. 2010;99(9):4023–4031.
- Flory PJ. Thermodynamics of dilute solutions of high polymers. J Chem Phys. 1945;13(11):453–465.
- 30. de Gennes PG, Scaling Concepts in Polymer Physics, Cornell University Press; 1979.
- Zhao Y, Inbar P, Chokshi HP, Malick AW, Choi DS. Prediction of the thermal phase diagram of amorphous solid dispersions by flory–huggins theory. J Pharm Sci. 2011;100(8):3196–3207.
- 32. Lodge TP, Hiemenz PC. Polymer Chemistry. 3 ed. CRC Press; 2020.
- 33. Daoud M, Cotton JP, Farnoux B, et al. Solutions of flexible polymers. neutron experiments and interpretation. *Macromolecules*. 1975;8(6):804–818.
- Sahoo A, Suryanarayanan R, Siegel RA. Stabilization of amorphous drugs by polymers: the role of overlap concentration (C\*). Mol Pharm. 2020;17(11):4401–4406.
- 35. Doi M, Edwards SF. The Theory of Polymer Dynamics. Clarendon Press; 1986.
- **36.** Song S, Wang C, Wang S, Siegel RA, Sun CC. Efficient development of sorafenib tablets with improved oral bioavailability enabled by coprecipitated amorphous solid dispersion. *Int J Pharm.* 2021;610:121216.
- 37. Rubinstein M, Colby RH. Polymer Physics. Oxford University Press; 2003.
- **38.** Flory PJ. Thermodynamics of crystallization in high polymers, IV. A theory of crystalline states and fusion in polymers, copolymers, and their mixtures with diluents. *J Chem Phys.* 1949;17(3):223–240.
- **39.** Wang K, Sun CC. Crystal growth of celecoxib from amorphous state: polymorphism, growth mechanism, and kinetics. *Cryst Growth Des.* 2019;19 (6):3592–3600.
- Tao J, Sun Y, Zhang GGZ, Yu L. Solubility of small-molecule crystals in polymers: d-mannitol in PVP, indomethacin in PVP/VA, and nifedipine in PVP/VA. *Pharm Res.* 2009;26(4):855–864.
- 41. Baird JA, Taylor LS. Evaluation of amorphous solid dispersion properties using thermal analysis techniques. *Adv Drug Deliv Rev.* 2012;64(5):396–421.
- 42. Andronis V, Yoshioka M, Zografi G. Effects of sorbed water on the crystallization of indomethacin from the amorphous state. *J Pharm Sci.* 1997;86(3):346–351.
- Gupta P, Thilagavathi R, Chakraborti AK, Bansal AK. Role of molecular interaction in stability of celecoxib—PVP amorphous systems. Mol Pharm. 2005;2(5):384–391.
- Wu T, Yu L. Surface crystallization of indomethacin below Tg. Pharm Res. 2006;23 (10):2350–2355.
- Li Y, Yu J, Hu S, et al. Polymer nanocoating of amorphous drugs for improving stability, dissolution, powder flow, and tabletability: the case of chitosan-coated indomethacin. Mol Pharm. 2019;16(3):1305–1311.
- **46.** Chen H, Pui Y, Liu C, et al. Moisture-induced amorphous phase separation of amorphous solid dispersions: molecular mechanism, microstructure, and its impact on dissolution performance. *J Pharm Sci.* 2018;107(1):317–326.